On the distribution and bonding environment of Zn and Fe in glasses containing electric arc furnace dust: A μ-XAFS and μ-XRF study

F. Pinakidou [a], M. Katsikini [a], E.C. Paloura [a,*], P. Kavouras [a],
Th. Kehagias [a], Ph. Komninou [a], Th. Karakostas [a], A. Erko [b]

[a] Aristotle University of Thessaloniki, Department of Physics, GR54124 Thessaloniki, Greece
[b] BESSY GmbH, Albert Einstein Street 15, 12489 Berlin, Germany

Abstract

We apply synchrotron radiation assisted X-ray fluorescence (SR-XRF), SR-XRF mapping as well as micro- and conventional X-ray absorption fine structure (μ-XAFS and XAFS) spectroscopies in order to study the bonding environment of Fe and Zn in vitrified samples that contain electric arc furnace dust from metal processing industries. The samples are studied in the as-cast state as well as after annealing at 900 °C. The SR-XRF results demonstrate that annealing does not induce any significant changes in the distribution of either Fe or Zn, in both the as-cast and annealed glasses. The μ-XAFS spectra recorded at the Fe-K and Zn-K edges reveal that the structural role of both Fe and Zn remains unaffected by the annealing procedure. More specifically, Fe forms both FeO_6 and FeO_4 polyhedra, i.e. acts as an intermediate oxide while Zn occupies tetrahedral sites.
© 2006 Elsevier B.V. All rights reserved.

Keywords: X-ray fluorescence spectroscopy; EXAFS; NEXAFS; μ-EXAFS; Electric arc furnace dust

1. Introduction

Electric arc furnace dust (EAFD) is one of the largest solid waste streams produced by steel mills, and is classified as a waste under the Resource Conservation and Recovery Act (RCRA) of the U.S. Environmental Protection Agency (EPA). Steel production by electric-arc furnace (EAF) technology has been of increasing importance over the past 20 years, and it is expected that, in the coming years, it will dominate the steel production. During the EAF production of steel, about 15–20 kg of dust is formed per tonne of steel. This dust contains heavy metals and thus is considered as a toxic waste. These metals are found both as free oxides (e.g. PbO, ZnO) as well as in the form of composite structures with iron oxides (e.g. $ZnFe_2O_4$). More specifically, EAF dusts contain iron, zinc, calcium and silicon in the form of simple or mixed oxides, as well as copper, manganese, chromium, cadmium and lead which either originate from the scrap iron raw material or are introduced as additives [1,2]. Successful recycling of the valuable metals (iron, zinc and lead) reduces the disposal problems and results in resource conservation. Hydrometallurgical or pyrometallurgical processes can recover only a part of heavy metals (such as Zn) from the EAFD [2,3] and hence it is of major importance to develop an additional process that stabilizes metallic Zn and the other heavy metals found in the residues of Zn recovery processes. One of the promising methods for safe disposal of the EAF dust is vitrification [4,5] that leads to the production of chemically stable materials, vitreous or glass-ceramic, that can be safely disposed or used for construction and decorative applications [6,7].

The aim of this work is to determine the distribution, the bonding environment and the oxidation state of Fe and Zn ions in the glass matrix of vitrified EAFD-rich industrial wastes. It is known that the structural role of Fe depends on its valence state [8,9]: Fe^{2+} acts as a glass modifier and participates in the formation of FeO_6 polyhedra while Fe^{3+} is an intermediate oxide, i.e. can also act as a glass network former by constituting FeO_4. On the contrary, in such oxide materials Zn is known to be stable only in its 2+ oxidation state and can occupy tetrahedral sites [10]. Therefore it is quite important to study the structural role of both Fe and Zn oxides, since the structural integrity of the glass

---

* Corresponding author. Tel.: +30 2310998036; fax: +30 2310998036.
E-mail address: paloura@auth.gr (E.C. Paloura).

matrix depends strongly on the type of polyhedra that the Fe and Zn ions form. It should be pointed out that the glass forming role of Fe depends also on the waste content [11]. Furthermore, heating at temperatures above the glass transition temperature can induce devitrification [12–14]. More specifically, annealing induced modifications in the bonding environment of Fe were previously reported in a series of Pb- and Fe-rich waste contaminated glasses [12].

In this paper we present the characterization of Fe- and Zn-rich solidified-stabilized EAFD glasses in the as-cast state as well after annealing by means of synchrotron assisted X-ray fluorescence (SR-XRF) mapping and X-ray absorption fine structure (XAFS) measurements at the Fe-K and Zn-K edges. SR-XRF mapping is a non-destructive characterization technique that permits the two-dimensional imaging of the distribution of different elements in an inhomogeneous sample with ppm detectability. The use of capillary optics reduces the beam size (in our set-up to 5 μm) and thus improves the spatial resolution. The XAFS spectrum, which shows the dependence of the X-ray absorption coefficient on the impinging photon's energy above the absorption edge of a specific element, consists of two regions: the extended X-ray absorption fine structure (EXAFS) region and near-edge extended X-ray absorption fine structure (NEXAFS) region. The former reflects the bonding environment (as that is determined by the nearest neighbour distances and coordination numbers) of the absorbing atom. The latter reflects the density of empty states of the absorbing atom and it is affected by the symmetry, the local coordination geometry and the valence of the absorbing atom, which can be derived by proper analysis of the NEXAFS spectra. Local changes in the bonding environment around Fe and Zn can be identified and mapped over selected areas of the sample using micro-XAFS (μ-XAFS).

2. Sample preparation and experimental details

The samples under study are vitrified products of EAF dust which mainly consists of zinc (34.9 wt.% ZnO) and ferric oxides (in the form of $ZnFe_2O_4$ at 33.9 wt.%). The elemental composition and the structural analysis of the EAF dust were performed using energy-dispersive X-ray spectrometry (EDS) and X-ray diffraction (XRD), respectively [15]. The loss on ignition (LOI) mass, as determined with EDS after the EAFD powder was heated to 1000 °C, amounts to 7.2 wt.% [15]. The two main constitutive oxides of EAFD are zinc ferrite ($ZnFe_2O_4$) and zinc oxide (ZnO), while traces of MgO, Al_2O_3, SiO_2, K_2O, CaO, MnO and PbO were also identified. The composition of the as-cast glass was determined by EDS analysis which revealed that the weight percentage of Fe, Zn, Ca, Na and Si is approximately 8.2, 6.7, 31.1, 12.6 and 50.0 wt.%, respectively. Details on the composition of the EAFD powder and the as-cast product are listed in Table 1.

The vitrification process involves mixing of the EAF dust with SiO_2, Na_2CO_3 and $CaCO_3$ powders and co-melting at 1400 °C for 2 h in a Pt-crucible, followed by quenching in air [11–15]. The sample under study consists of 20 wt.% EAFD, 55 wt.% SiO_2, 15 wt.% CaO and 10 wt.% Na_2O. After quenching the sample was heated at a temperature 20 °C above the glass

Table 1
Composition of EAFD powder and as-cast product as determined by EDS

EAFD powder		As-cast product	
Compound	wt.% (±1%)	Element	wt.% (±1%)
MgO	0.7	Si	50.0
Al_2O_3	0.9	Ca	21.1
SiO_2	4.1	Mn	1.4
K_2O	1.4	Fe	8.2
CaO	4.6	Zn	6.7
MnO	3.3	Na	12.6
Fe_2O_3	33.9		
ZnO	34.9		
PbO	6.2		
LOI	7.2		
Humidity	2.0		

transition temperature ($T_g = 583.8$ °C) for residual stress relaxation. Next, the sample was subjected to a two-stage isothermal treatment process (annealing). In the first stage (20 min at 680 °C), nucleation of wollastonite $CaSiO_3$ takes place and in the second (30 min at 900 °C) crystal growth occurs [15]. The temperatures for the annealing process were determined from the differential thermal analysis results reported previously [15]. Recently reported transmission electron microscopy (TEM) observations and XRD analysis showed that the initial product was amorphous while EDS analysis revealed that all elements were homogeneously dispersed into the vitreous matrix [15]. Furthermore, upon annealing surface crystallization of wollastonite ($CaSiO_3$) initiates from the edges towards the center [15].

The XRF, XAFS and μ-XAFS measurements were conducted at the KMC2 beamline at the synchrotron radiation (SR) facility BESSY in Berlin. The beamline is equipped with a double-crystal monochromator and capillary optics that reduce the beam diameter to 5 μm. The XRF spectra were recorded with acquisition time 400 s. The XRF maps were recorded using excitation photons of 9600 eV, i.e. higher than the Fe-K and Zn-K absorption edges and acquisition time 1 s/point. The angle of incidence of the SR beam was 45° and the energy dispersive (Röntec) fluorescence detector was positioned normal to the beam. The Fe-K and Zn-K edge fluorescence photons emitted from the sample were discriminated by setting electronically the energy range of interest from 6097 to 7181 eV and 8037–9092 eV, respectively. The μ-XAFS spectra (beam diameter 5 μm) were recorded at the Fe-K and Zn-K edges, in the fluorescence yield mode, at two spots: one at the edge (position E) and the other at the centre (position C) of the annealed sample. Measurement at two spots was decided because, according to previous reports [15], the crystallization of wollastonite starts at the edges and progresses towards the centre of the sample. Therefore local inhomogeneities might occur across the sample surface. The spectrum of the Fe_2O_3 reference sample was recorded in the transmission mode using ionization chambers. The conventional EXAFS spectra (capillary removed, beam size 200 μm × 800 μm) for the as-cast and annealed samples were recorded at the Fe-K and Zn-K edges in the fluorescence yield mode using a Si-PIN pho-

todiode. Energy calibration was performed using the absorption edge position of the spectrum of a Fe foil. Hereafter, the spectra recorded with the capillary optics are denoted with the prefix micro (μ-). Finally, a powder hematite sample (alpha-Fe_2O_3) is used as reference for the XAFS measurements.

3. Results and discussion

3.1. SR-XRF results

SR-XRF spectra from the as-cast and annealed samples were used in order to identify possible local variations in the distribution of Fe and Zn. The spectra shown in Fig. 1 were recorded with excitation energy equal to 9600 eV, i.e. high enough to excite Kα and Kβ photons from both Fe and Zn. Among the spectra, those recorded from the edge and the center of the sample are μ-SR-XRF. As shown in the spectra, the samples under study contain Fe, Zn, Ca and Mn, while the presence of Si and Na, that also exist in the glass, is not detected due to the high excitation energy and the resulting low absorption cross-section for low Z elements. In order to quantify annealing-induced changes in the sample composition, the XRF spectra were fitted with Gaussian functions that simulate the Fe-Kα, Fe-Kβ and Zn-Kα emission lines (at 6.34, 7.04 and 8.61 keV, respectively). More specifically, the concentration ratio of Fe versus Zn (C_{Fe}/C_{Zn}) can be calculated using the expression $C_{Fe}/C_{Zn} = ((Q_{Fe}\omega_{Fe}\alpha_{Fe})/(Q_{Zn}\omega_{Zn}\alpha_{Zn}))(I_{Fe}/I_{Zn})$ [16], where Q_i is the absorption cross-section of element i for incident photon energy equal to 9600 eV, ω_i the fluorescence yield of the Kα emission lines of element i and α_i is the Kα transition probability of element i. The error in the determination of the elements' concentration was evaluated from the least square fitting method. The analysis of the XRF spectra reveals that the C_{Fe}/C_{Zn} concentration ratio at the edge and center of the annealed product is equal to 1.90 ± 0.01 and 1.94 ± 0.01 respectively, i.e. practically equal between the two spots. This observation indicates that the formation of either Fe- or Zn-rich regions has been avoided in accordance with Kavouras et al. [15].

The homogeneous distribution of Fe and Zn over rather large areas of the samples is depicted in the XRF maps shown in
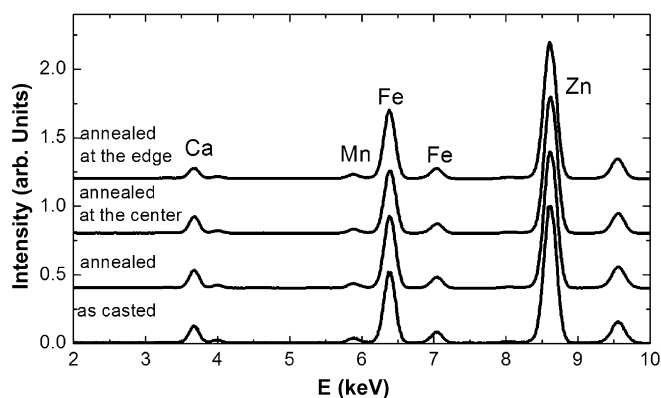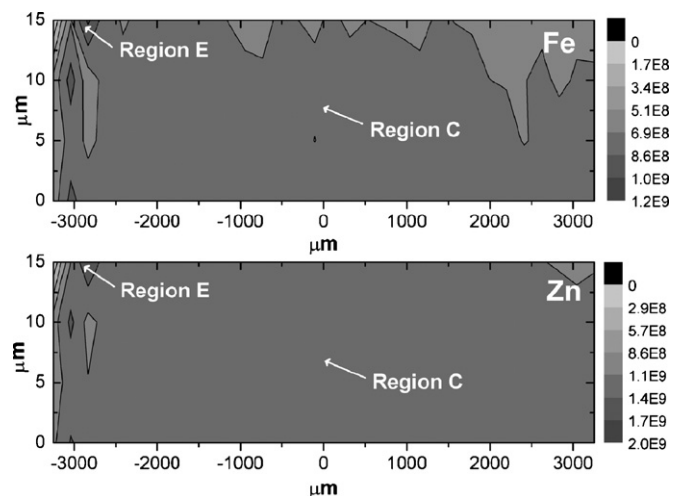
Fig. 2. The 7500 μm × 15 μm μ-SR-XRF maps of the distribution of Fe and Zn in the annealed sample. The regions depicted as E and C, refer to the positions at the edge and at the centre of the annealed sample, respectively.

Fig. 2. The maps have dimensions 6200 μm × 15 μm and reveal that the distribution of Fe and Zn is rather homogeneous and formation of Fe and Zn clusters has been avoided.

3.2. EXAFS and μ-EXAFS results

The EXAFS and μ-EXAFS spectra were recorded at the Fe- and Zn-K edges at room temperature. In order to avoid self-absorption effects the EXAFS spectra were recorded at near normal incidence ($\theta = 85°$ to the sample surface). However, due to geometrical limitations set by the capillary optics the μ-EXAFS spectra were recorded at $\theta = 45°$ and were corrected for self-absorption phenomena [17]. Prior to analysis, the EXAFS and μ-EXAFS spectra were subjected to subtraction of the atomic absorption using the AUTOBK program [18] and corrected for monochromator-induced energy shifts using the spectrum of a Fe foil. The model for the fitting was constructed using the FEFF8.0 [18] program. The Fourier transforms (FT) of the k^3-weighted EXAFS spectra at the Fe- and Zn-K edges are shown in Fig. 3(a) and (b), respectively. The FT was calculated in the k-range 2.5–9.3 Å^{-1} for both the Fe- and Zn-K edges. As shown in the figure, the FTs of the samples under study have well-resolved structure up to a distance of about 3.5 Å from the absorbing atom. Therefore, mid-range order exists around both the Fe and Zn ions, possibly in the form of nanocrystallites which are not resolved in the XRF maps due to their small size (smaller than the 5 μm resolution limit set by the capillary optics).

The errors in the determination of the nearest neighbour distances and coordination numbers in the Zn-K EXAFS analysis were calculated using different spline functions for the subtraction of the atomic absorption background. These errors are equal to 10, 20 and 30% and ± 0.01 Å, ± 0.02 Å and ± 0.03 Å in the first, second and third nearest-neighbour (nn) shells, respectively. In the case of the Fe-K edge spectra, where the mixed model is used, some of the parameters were kept fixed (i.e. Debye–Waller factors and Fe–O bondlength of tetrahedrally coordinated Fe) in order to eliminate the error introduced in the determination of

Fig. 1. Fluorescence spectra normalized at the Zn-Kα peak, recorded at the edge and the centre of the annealed sample (μ-SR-XRF) and at random positions of the as-cast and annealed sample.
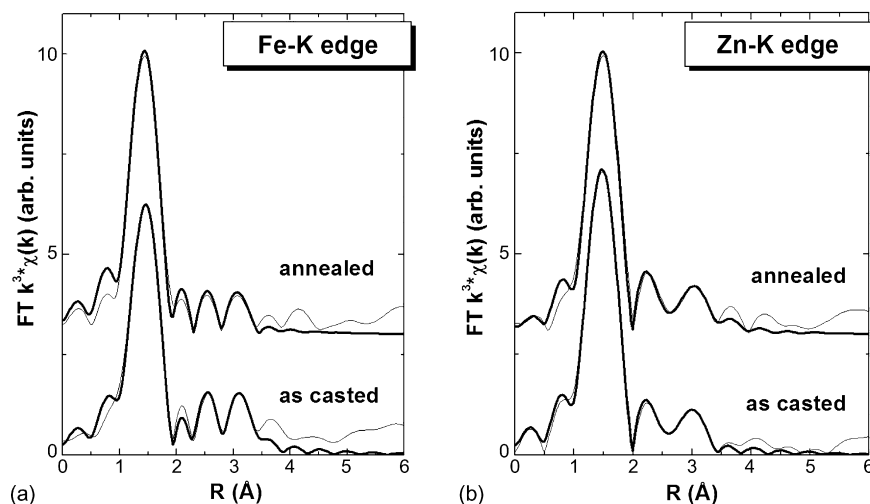
Fig. 3. Fourier transforms of the EXAFS spectra recorded at the (a) Fe-K and (b) Zn-K edge, respectively. The raw data and the fitting are shown in thin and thick solid lines, respectively.

percentage of the FeO_x polyhedra. The error bars used are those determined by the FEFFIT program [18].

Given that Fe can act as either a modifier or an intermediate, by constituting FeO_6 octahedra and/or FeO_4 tetrahedra respectively, we chose to fit the Fe-K edge EXAFS spectra using a mixed model according to which $X\%$ of the Fe ions occupy octahedral sites, that belong to the $ZnFe_2O_4$ phase (which exists in the EAF dust), while $(1 - X)\%$ form tetrahedra, and participate in the formation of the glass. In both the as-cast and annealed samples, the fitting procedure was performed using four shells: the first nearest neighbour (nn) shell consists of oxygen ions that are either octahedrally or tetrahedrally coordinated to the Fe atom. The second, third and forth nn shells are comprised of Fe, Zn and O ions, according to the $ZnFe_2O_4$ model. The Zn-K EXAFS spectra were fitted using the $ZnFe_2O_4$ model and the fitting procedure was performed assuming four shells: in the first nn shell Zn is tetrahedrally coordinated with four oxygen ions while the second, third and fourth shells comprise of Fe, O and Zn ions, respectively. During the fitting of the Fe-K edge

spectra, where the mixed model is used, some of the parameters were kept fixed (i.e. Debye–Waller factors and Fe–O bondlength of tetrahedrally coordinated Fe) in order to reduce the error in the determination of percentage of the FeO_x polyhedra. This choice does not degrade the quality of the presented results but instead improves the accuracy. More specifically, we chose to keep the Fe–O distance in the FeO_4 units constant because this bond length is expected to vary in the narrow range 1.86–1.88 Å [19,20]. Contrary to that the Fe–O bond length in the FeO_6 units can vary over the broader range 1.92–2.10 Å [19,20]. Therefore since we do not expect any significant changes in the Fe–O distance in the FeO_4 units we chose to keep this distance fixed and iterate for Fe–O in the FeO_6 octahedra thus reducing the number of iterated parameters during the fitting. The analysis of the spectra from the hematite reference sample reveals the expected trigonal distortion of the FeO_6 octahedron, which causes a splitting of the first nearest neighboring shell (three oxygen ions at 1.93 Å and three oxygen ions at 2.09 Å, respectively) [21]. The results of the EXAFS and μ-EXAFS analysis are listed in Table 2.

Table 2
EXAFS and μ-EXAFS results for the Fe-K and Zn-K edges

Samples	Fe-K edge			Zn-K edge		
	Percentage (%) of FeO_x	$R_{Fe–O}$ (± 0.01 Å)	DW ($\times 10^{-3}$ Å)	N (O) (10%)	$R_{Zn–O}$ (± 0.01 Å)	DW ($\times 10^{-3}$ Å)
EXAFS						
As-cast	$FeO_6 = 51$ ($\pm 4\%$)	1.86	2	4.3	1.94	4.4
	$FeO_4 = 49$	1.95	3.1			
Annealed at 900 °C	$FeO_6 = 47$ ($\pm 6\%$)	1.86*	2*	4.1	1.94	3.7
	$FeO_4 = 53$	1.92	3.1*			
μ-EXAFS						
Annealed at the edge	$FeO_6 = 69$ ($\pm 10\%$)	1.86*	2*	4.2	1.94	5.4
	$FeO_4 = 31$	1.92	3.1*			
Annealed at the center	$FeO_6 = 57$ ($\pm 7\%$)	1.86*	2*	4.1	1.94	3.9
	$FeO_4 = 43$	1.94	3.1*			

The symbols N and R indicate the coordination numbers and interatomic distances in the first nearest-neighbour shell. The asterisk (*) indicates parameters that were kept fixed during the analysis.

As shown in the table, in both the as-cast and annealed sample, about 50% of the Fe ions are tetrahedrally coordinated with oxygen ions while the rest 50% form octahedra. The corresponding Fe–O distances, which are characteristic of tetrahedral and octahedral coordination [19,20], are 1.86 and 1.93 Å, respectively. It has been previously reported that the reduction of Fe^{3+} to Fe^{2+} can happen during melting in iron-silicate glasses when the concentration of Fe in the melt is below 5 mol% [22]. Such a reduction cannot be directly detected in the EXAFS spectra. In addition, previous work on iron silicate glasses suggested that it is possible that Fe^{2+} ions can occupy tetrahedral sites in the glass matrix [23,24]. However when Fe^{2+} ions constitute tetrahedra, the Fe–O bondlength in the FeO_4 polyhedra (1.99 Å [22]) is expected to be significantly longer than the respective in the FeO_4 of Fe^{3+} ions (1.865 Å [20,22]). Hence, if we take into account that only Fe^{3+} ions can constitute both tetrahedra and octahedra with such short Fe–O bondlengths [22] into the glass matrix we can conclude that the observed alteration in the Fe–O bondlength can only be attributed to Fe^{3+} ions. Hence, Fe^{3+} participates in the formation of the vitreous matrix by constituting FeO_4 and FeO_6 polyhedra, i.e. the intermediate role of the Fe^{3+} oxide is revealed. As far as the second and third nn shells are concerned, in both the as-cast and annealed samples, the Fe and Zn ions occupy sites at distances 2.99 and 3.35 Å, from the central Fe atom, respectively. Therefore, it can be concluded that annealing does not cause any major changes in the bonding environment of Fe.

The EXAFS analysis at the Zn-K edge reveals that the bonding environment around the Zn atom is not affected by annealing. In both the as-cast and annealed samples, the Zn atom is coordinated with four oxygen ions at a distance 1.94 Å. The second nn shell is found to consist of approximately 12 Fe ions at a distance of 3.35 Å, i.e. in agreement with the $ZnFe_2O_4$ model. Finally, the Zn–O distance in the third nn shell ranges from 3.53 to 3.46 Å (the coordination number is not discussed since the determined changes are within the 30% error bar of the EXAFS analysis in the third nearest neighbour shell).

In order to investigate possible changes in the bonding environment due to local compositional variations as well as due to differences in the cooling rate between the center and at the edge of the samples, we resorted to μ-EXAFS spectra recorded at the Fe-K and Zn-K edges, from two spots of the sample surface: spot E corresponds to the edge of the sample annealed at 900 °C while spot C corresponds to the center of the same sample (hereafter denoted as E and C, respectively). The Fourier transforms (FTs) of the k^3-weighted μ-EXAFS spectra recorded at the Fe- and Zn-K edges are shown in Fig. 4(a) and (b), respectively. The FTs were calculated in the k-range 2.7–9.3 and 2.5–9.3 $Å^{-1}$ for the Fe- and Zn-K edges, respectively. In accordance with the EXAFS analysis, the existence of mid-range order around both the Fe and Zn ions is again evident in the FTs.

The Fe- and Zn-K μ-EXAFS spectra were fitted using the same models applied for the analysis of the EXAFS spectra. The analysis of the μ-EXAFS spectra from the annealed sample (Table 2) reveals that the percentage of the Fe ions that constitute octahedra is, within the error bar, equal at the center and at the edge of the sample. More specifically, 69% of the Fe ions form octahedra at the edges of the sample, while 57% form octahedra at the center of the sample. The Fe–O bond length in the FeO_6 polyhedron is equal to 1.93 Å whilst the respective value in the FeO_4 tetrahedron is 1.86 Å. Therefore, the μ-EXAFS results verify that the intermediate role of Fe is retained, i.e. Fe participates in the formation of the vitreous matrix by forming FeO_4 tetrahedra and acts as a glass modifier when bonded in FeO_6 octahedra. As far as the second and third nn shells are concerned, we detect a small distortion around Fe at the center of the sample, i.e. the $R_{Fe–Fe}$ and $R_{Fe–Zn}$ distances are 2.92 and 3.16 Å at the center and 2.99 and 3.60 Å at the edge, respectively. The Fe ions that occupy octahedral sites belong to $ZnFe_2O_4$ nanocrystallites, which are not resolved in the XRF maps due to the limited spatial resolution of the experimental set-up. In particular, the lateral resolution of the XRF maps is limited by the beam dimension provided by the available capillary optics which in the present case is 5 μm (without the capillary the beam dimensions are 200 μm × 800 μm). Therefore, if nanocrystallites with smaller
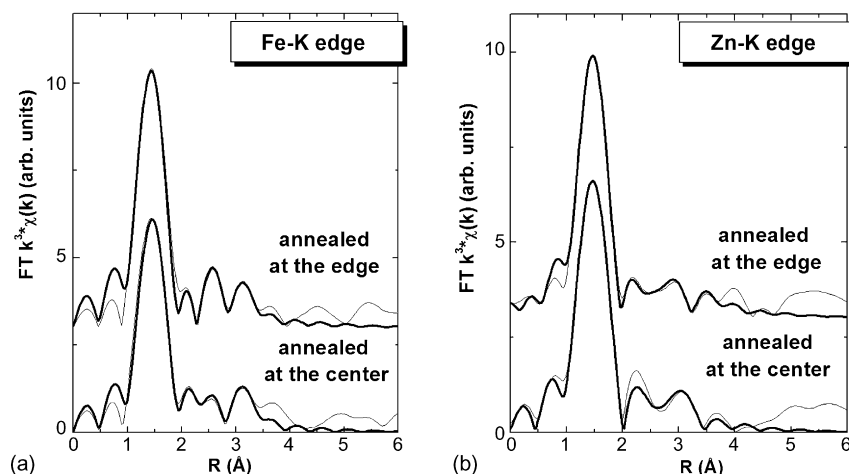

Fig. 4. Fourier transforms of the (a) Fe-K and (b) Zn-K edge μ-EXAFS spectra recorded at the edge and at the centre of the annealed sample. The raw data and the fitting are shown in thin and thick line, respectively.

dimensions than 5 μm exist, they will not be imaged in the XRF maps. On the other hand, EXAFS is not limited by the beam dimensions, thus it is more sensitive and the presence of well-resolved structure at distances beyond the first nn shell, as it is the case in our spectra, is the signature of nanostructure. The presence of zinc ferrite nanocrystallites in an amorphous silica matrix has been previously reported in sol–gel materials [25]. More specifically, Zhou et al. reported that upon annealing at 900 °C, the glass structure was preserved and zinc ferrite crystallites of ~3 nm sizes were uniformly dispersed in the amorphous silica matrix.

Finally, the μ-EXAFS analysis at the Zn-K edge reveals that the bonding environment of the Zn atom is the same in both the centre and the edge of the annealed sample. More specifically, in both regions, the Zn atom participates in the formation of ZnO_4 tetrahedra, i.e. Zn is coordinated with four oxygen ions at a distance 1.94 Å. The characteristics of the higher shells are, within the error bar, identical to those determined from the EXAFS analysis discussed earlier. Therefore, the bonding environment of Zn is invariant in different regions of the annealed sample.

3.3. μ-NEXAFS and NEXAFS results

The Fe-K NEXAFS and μ-NEXAFS spectra of the samples under study and the reference Fe_2O_3 compound are shown in Fig. 5(a) (the spectra from the center and the edge of the sample were recorded in the μ-NEXAFS mode). The NEXAFS spectra of Fe-containing compounds are characterized by a pre-edge peak that is attributed to $1s \rightarrow 3d$ transitions [26]. In a centrosymmetric environment (e.g. octahedral) the intensity of the pre-edge peak is weak due to the quadrupole character of the transition. Contrary to that, in a non-centrosymmetric environment (e.g. tetrahedral) the pre-edge peak gains intensity due to the d–p mixing of the final state that gives dipole character to the transition. Thus, the intensity of the pre-edge peak is inversely proportional to the coordination number of the absorbing atom due to the loss of inversion symmetry of the iron site [27,28]. Not only the intensity but also the shape of the pre-edge peak depends on the local coordination around Fe. According to Westre et al.

[29], fitting of the pre-edge peak with one Lorentzian is a fingerprint of the tetrahedral coordination of the Fe ions. Contrary to that, two Lorentzians are necessary to fit the pre-edge peak when Fe occupies octahedral sites. Finally, it should be mentioned that the position of the pre-edge peaks is a measure of the portion of various oxidations states of Fe in a mixed valence sample, i.e. the $Fe^{3+}/\Sigma Fe$ ratio, and depends on the bonding environment of the Fe atom [30].

Prior to analysis the spectra were normalized for the transmission function of the monochromator and were subjected to linear background subtraction (by fitting the spectrum far before the absorption edge) and normalization to the edge jump. The characteristics of the Fe-K and Zn-K NEXAFS spectra were determined via fitting using a sigmoidal (Boltzmann function) to simulate transitions to the continuum and Gaussians to simulate transitions to bound states [31]. The pre-edge peak in the Fe-K edge NEXAFS spectra was fitted using Lorentzians.

The presence of the pre-edge peak in the NEXAFS spectra of all the samples under study indicates that the polyhedron around Fe is either a tetrahedron and/or an asymmetric octahedron. In the reference hematite (Fe_2O_3) sample, where Fe belongs to a distorted octahedral environment, two Lorentzians (centered at 7113.5 and 7116.8 eV, respectively) were necessary to fit the pre-edge region. Contrary to that the pre-edge peak in the spectra of the studied samples was fitted using one Lorentzian. It should be pointed out that, in the case of a mixed bonding environment (both octahedral and tetrahedral), due to the weak contribution of the centrosymmetric environment, one Lorentzian would be adequate to fit the pre-edge peak. Therefore, in the case of the studied samples, the use of one Lorentzian is an indication that the Fe either belongs to a tetrahedral environment or a mixed octahedral/tetrahedral bonding environment. However, if we take into account the EXAFS results, it becomes clear that in the studied samples the use of one Lorentzian signifies that the Fe atom is coordinated both octahedrally and tetrahedrally with oxygen ions. Finally, the energy position of the pre-edge peak (centered at 7113.2 ± 0.2 eV), which depends on the oxidation state of Fe, is the same in all the samples indicating that the $Fe^{3+}/\Sigma Fe$ ratio remains constant in all vitrified products, i.e. is unaffected by
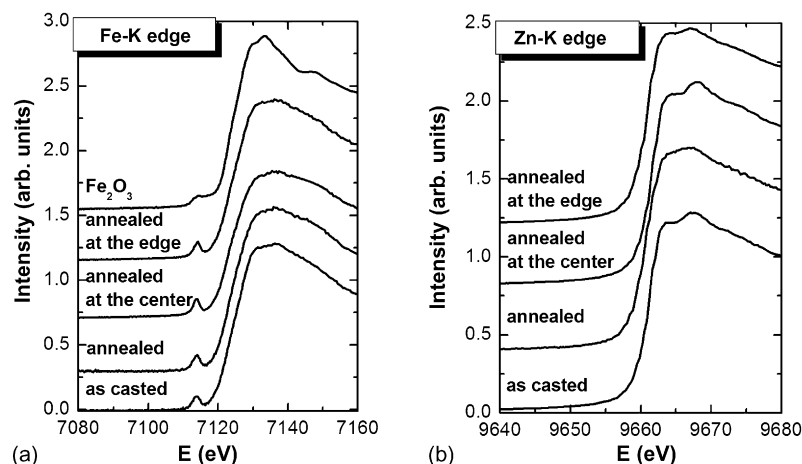

Fig. 5. The (a) Fe-K edge and (b) Zn-K edge μ-NEXAFS and NEXAFS spectra from the as-cast and annealed sample. The spectra from the annealed sample were recorded at the edge (μ-NEXAFS), at the centre (μ-NEXAFS) and at a random position. The spectrum of the reference Fe_2O_3 is also included in (a).

annealing and is invariant in different positions of the annealed sample. It should be pointed out that, even though the reduction of Fe^{3+} to Fe^{2+} cannot be excluded, the overall reduction of the Fe^{3+} would cause a shift of the position of the pre-edge peak of about 0.2 eV [30] which is of the order of the resolution of the NEXAFS spectra (± 0.2 eV) and thus cannot be evaluated.

The energy position of the absorption edge (E_{abs}), in the samples under study is equal to that in hematite (7122.2 eV). According to Salem et al. [32], the E_{abs} is a fingerprint of the valence of the absorbing atom and can be affected by modifications in the ionicity of the Fe–O bond and the symmetry (bondlength and coordination) around the Fe atom. Since we did not detect any energy shifts, it is affirmed that no alteration in the parameters mentioned above occurs, in agreement with the EXAFS analysis.

The NEXAFS and μ-NEXAFS spectra recorded at the Zn-K edge are shown in Fig. 5(b). The spectra have structure at energies above the absorption edge (E_{abs}), which indicates that the material is nanocrystalline around the Zn atom in accordance with the results of Zhou et al. [25].

4. Conclusions

SR-XRF mapping of vitrified EAF dust reveals that the annealing at $900\,^{\circ}$C does not alter the distribution of Fe and Zn in the studied samples. According to the EXAFS results the environment around the Fe atom is mixed, i.e. Fe forms FeO_4 tetrahedra that link to the vitreous matrix, while it also occupies octahedral sites in $ZnFe_2O_4$ nanocrystallites. The Fe–O distance is found equal to 1.93 and 1.86 Å for tetrahedrally and octahedrally coordinated Fe, respectively. Therefore, Fe participates in the formation of the glassy network acting as an intermediate oxide. Annealing does not affect the concentration of FeO_6 and thus does not modify the structural role of Fe. On the other hand, Zn occupies tetrahedral sites in both the as-cast and annealed sample, i.e. annealing does not affect its bonding environment. Finally, analysis of μ-EXAFS recorded from different spots of the samples under study reveals that there are no detectable local changes in the bonding environment of either Fe or Zn.

Acknowledgements

References

[1] T. Solifić, A. Rastovčan-Mioč, Š. Cerjan-Stefanović, V. Novosel-Radović, M. Jenko, Characterization of steel mill electric-arc furnace dust, J. Hazard. Mater. 109 (2004) 59–90.

[2] N. Leclerc, E. Meux, J.M. Lecuire, Hydrometallurgical recovery of zinc and lead from electric arc furnace dust using mononitrilotriacetate anion and hexahydrated ferric chloride, J. Hazard. Mater. 91 (2002) 257–270.

[3] R. Sekula, M. Wnek, A. Selinger, M. Wrobel, Electric arc furnace dust treatment: investigation on mechanical and magnetic separation methods, Waste Manage. Res. 19 (2001) 271–275.

[4] P. Pisciella, S. Crisucci, A. Karamanov, M. Pelino, Chemical durability of glasses obtained by vitrification of industrial wastes, Waste Manage. 21 (2001) 1–9.

[5] M. Pelino, A. Karamanov, P. Pisciella, S. Criscussi, D. Zonetti, Vitrification of electric arc furnace dusts, Waste Manage. 22 (2002) 945–949.

[6] L. Barbieri, A. Corradi, I. Lancellotti, Bulk and sintered glass-ceramics by recycling municipal incinerator bottom ash, J. Eur. Ceram. Soc. 20 (2000) 1637–1643.

[7] J. Sheng, Vitrification of borate waste from nuclear power plant using coal fly ash. II. Leaching behaviour of the FA30 glass, Fuel 81 (2002) 253–256.

[8] F. Pinakidou, M. Katsikini, E.C. Paloura, P. Kavouras, Ph. Komninou, T. Karakostas, A. Erko, XAFS studies on vitrified industrial waste, Phys. Scripta 351 (2005) 2474–2480.

[9] G. Lusvardi, L. Malavasi, L. Menabue, M.C. Menziani, Synthesis, characterization and molecular dynamics simulation of Na_2O–CaO–SiO_2–ZnO glasses, J. Phys. Chem. B 106 (2002) 9753–9760.

[10] A.B. Rosental, S.H. Grofalini, Molecular dynamics simulation of amorphous zinc silicate, J. Non-Cryst. Solids 87 (1986) 254–562.

[11] F. Pinakidou, M. Katsikini, E.C. Paloura, P. Kavouras, O. Kalogirou, Ph. Komninou, Th. Karakostas, On the coordination environment of Fe- and Pb-rich solidified industrial waste: an X-ray absorption and Mössbauer study, J. Non Cryst. Solids 352 (2006) 2933–2942.

[12] F. Pinakidou, M. Katsikini, E.C. Paloura, P. Kavouras, Ph. Komninou, Th. Karakostas, A. Erko, Study of annealing induced devitrification of stabilized industrial waste glasses by means of micro X-ray fluorescence mapping and absorption fine structure spectroscopy, J. Non Cryst. Solids 351 (2005) 2474–2480.

[13] P. Kavouras, G. Kaimakamis, T.A. Ioannidis, T. Kehagias, Ph. Komninou, S. Kokkou, E. Pavlidou, I. Antonopoulos, M. Sofoniou, A. Zouboulis, C.P. Hadjiantoniou, G. Nouet, A. Prakouras, Th. Karakostas, Vitrification of lead-rich solid ashes from incineration of hazardous industrial wastes, Waste Manage. 23 (2003) 361–371.

[14] P. Kavouras, Ph. Komninou, K. Chrissafis, G. Kaimakamis, S. Kokkou, K. Paraskevopoulos, Th. Karakostas, Microstructural changes of processed vitrified solid waste products, J. Eur. Ceram. Soc. 23 (2003) 1305–1311.

[15] P. Kavouras, I. Tsilika, Th. Kehagias, K. Chrissafis, G. Kaimakamis, D. Papadopoulos, S. Kokkou, Ph. Komninou, Th. Karakostas, Glass-ceramic materials obtained by crystallization of vitrified electric arc furnace dust, J. Hazard. Mater., in press.

[16] K. Janssens, L. Vincze, B. Vekemans, in: H.A. Koen, Janssens, C.V. Freddy, Adams, Anders Rindby (Eds.), Microscopic X-Ray Fluorescence Analysis, John Wiley & Sons, New York, 2000, pp. 155–210.

[17] L. Tröger, D. Arvanintis, K. Baberschke, H. Michaelis, U. Grimm, E. Zschech, Full correction of the self-absorption in soft-fluorescence extended X-ray-absorption fine-structure, Phys. Rev. B 46 (1992) 3283–3289.

[18] J. Mustre de Leon, J.J. Rehr, S.I. Zabinsky, R.C. Albers, Ab initio curved-wave X-ray-absorption fine structure, Phys. Rev. B 44 (1991) 4146–4156.

[19] M.D. Dyar, A review of Mössbauer data on inorganic glasses: the effects of composition on iron valency and coordination, Am. Mineral. 70 (1985) 304–316.

[20] Z. Yu, D.E. Day, G.J. Long, R.K. Brow, Properties and structure of sodium-iron phosphate glasses, J. Non-Cryst. Solids 215 (1997) 21–31.

[21] R.W.G. Wyckoff, Crystal Structures, vol. 2, 2nd ed., John Wiley & Sons, New York, 1964.

[22] D. Holland, A. Mekki, I.A. Gee, C.F. McConville, J.A. Johnson, C.E. Johnson, P. Appleyard, M. Thomas, The structure of sodium iron silicate glass—a multi-technique approach, J. Non-Cryst. Solids 253 (1999) 192–202.

[23] P.A. Bingham, J.M. Parker, T. Searle, J.M. Williams, K. Fyles, Redox and clustering of iron in silicate glasses, J. Non-Cryst. Solids 253 (1999) 203–209.

[24] K.F.E. Williams, C.E. Johnson, M.F. Thomas, Mossbauer spectroscopy measurement of iron oxidation states in float composition silica glasses, J. Non-Cryst. Solids 226 (1998) 19–23.

[25] Z.H. Zhou, J. Wang, J.M. Xue, H.S.O. Chan, Cluster glass structure in nanohybrids of nonstoichiometric zinc ferrite in silica matrix, Appl. Phys. Lett. 79 (2001) 3167–3169.

[26] Z. Wu, D.C. Xian, C.R. Natoli, A. Marcelli, E. Paris, A. Mottana, Symmetry dependence of X-ray absorption near-edge structure at the metal K edge of 3d transition metal compounds, Appl. Phys. Lett. 79 (2001) 1918–1920.

[27] G. Calas, J. Paetiau, Coordination of iron in oxide glasses through high-resolution K-edge spectra: information from the pre-edge, Solid State Commun. 48 (1983) 625–629.

[28] C.R. Randall, L. Shu, Y.M. Chiou, K.S. Hagen, M. Ito, N. Kitajima, R.J. Lachicotte, Y. Zang, L. Que, X-ray-absorption pre-edge studies of high-spin iron(II) complexes, Inorg. Chem. 34 (1995) 1036–1039.

[29] T. Westre, P. Kennepohl, J.G. DeWitt, B. Hedman, K.O. Hodgson, E.I. Solomon, A multiplet analysis of Fe K-edge 1s $\rightarrow$ 3d pre-edge features of iron complexes, J. Am. Chem. Soc. 119 (1997) 6297–6314.

[30] S. Bajt, S.R. Ruton, J. Delabey, X-ray microprobe analysis of iron oxidation-states in silicates and oxides using X-ray-absorption near-edge structure (XANES), Geochem. Cosmochem. Acta 58 (1994) 5209–5214.

[31] J. Stöhr, NEXAFS Spectroscopy, Springer-Verlag, Berlin, 1992.

[32] S.I. Salem, C.N. Chang, P.L. Lee, V. Severson, Energy shift of the K-absorption edge of Mn and Fe compounds, J. Phys. C: Solid State Phys. 11 (1978) 4085–4093.